J Solid State Electrochem (2012) 16:1651–1661
DOI 10.1007/s10008-011-1580-8

ORIGINAL PAPER

Electroactive porous films of myoglobin within calcium alginate

Qianqian Li · Hong Sun · Xingchao Liu · X. S. Zhao

Received: 18 May 2011 / Revised: 16 October 2011 / Accepted: 17 October 2011 / Published online: 6 November 2011

Abstract In this work, a novel two-step construction strategy for protein assembly films was proposed. The first step was the preparation of porous calcium alginate (CA) films by spraying calcium chloride ($CaCl_2$) solution over the mixture surface of sodium alginate and polyethylene glycol on various solid substrates. The second step involved the cast of myoglobin (Mb) onto the porous CA films and then formed the electroactive porous Mb-CA films. The nitrogen adsorption desorption isotherm, scanning electron microscope, alternating current impendence and cyclic voltammetry were used to characterize the porous films. Fully hydrated porous CA films had nearly 90 wt% water contents and UV–vis showed that Mb in the porous films retained its near native conformation at medium pH. The stable films modified on glassy carbon electrode demonstrated good electroactivity in protein-free buffer, which was originated from protein heme Fe(III)/Fe(II) redox couples. The electrochemical parameters such as apparent heterogeneous electron transfer rate constant (k_s) and formal potential ($E^{o\prime}$) were estimated by fitting the data of square-wave voltammetry with nonlinear regression analysis. It was observed that the formal potential of the Mb Fe (III)/Fe(II) couple in porous CA films shifted linearly between pH 4.0 and 11.0 with a slope of −52.7 mV/pH, suggesting that one proton transfer was coupled to each electron transfer in the electrochemical reaction. The porous Mb-CA films showed the electrocatalytic activity toward dioxygen, hydrogen peroxide, and nitrite with significant decreases in the electrode potential required, and exhibited good operational and storage stability, reproducibility and fast response time for H_2O_2 detection. It is showing the possible future application of the films for biosensors and biocatalysis.

Keywords Myoglobin · Porous calcium alginate films · Direct electrochemistry · Electrocatalysis

Q. Li · H. Sun (✉) · X. S. Zhao
Institute of Multifunctional Materials (IMM), Laboratory of New Fiber Materials and Modern Textile, College of Chemistry, Chemical Engineering and Environment, Qingdao University, Qingdao 266071, China
e-mail: sun_hong@qdu.edu.cn

X. Liu
Qingdao Qiushi Career College, Qingdao 266108, China

X. S. Zhao
School of Chemical Engineering, University of Queensland, St Lucia, Brisbane, QLD 4072, Australia

Introduction

Research on protein-containing or enzyme-containing thin films on electrode surfaces is largely driven by their potential applications in fabricating biosensors, biomedical devices, and enzymatic bioreactors [1, 2]. Achieving direct electron exchange between the protein and the electrode simplifies these devices by removing the requirement of chemical mediators, thus is of significance in fabricating the third-generation biosensors [3]. Direct electrochemistry of redox proteins can also provide a model for the mechanistic study of electron transfer between the enzymes in real biological systems. Thin films on electrodes may provide a favorable microenvironment for the proteins to directly exchange electrons with the underlying electrode, thus affording opportunities for investigating the enzyme electrochemistry [4–6].

Over the past decade, many protein film systems have been described [7]. Successful approaches include cast films of proteins with insoluble surfactants [8], hydrogel polymers [9–11], clay nanoparticle [17], polyelectrolyte- or clay-surfactant composites films [12–16]. All these films have been found to effectively enhance the direct electron transfer between the heme proteins and electrodes compared to that on bare electrodes with the proteins in solution.

Recently, there has been an increasing interest in using natural polymers as an enzyme immobilization matrix for biosensors. Sodium alginate (SA) is a natural ionic polysaccharide from seaweed plants. Due to its many desirable properties, such as low cost, chemical inertness and good film-forming ability, SA has been used in various practical fields [18, 19]. A distinct advantage of SA in fabricating biosensors is its biocompatibility and non-toxicity. Proteins such as hemoglobin [20] have been successfully immobilized on sodium alginate multi-walled carbon nanotubes composite films on electrodes for sensor applications. Myoglobin in SA film on a $BMIMPF_6$-modified carbon paste electrode surface also displayed good cyclic voltammetry response and electrocatalysis [21].

SA is a family of unbranched binary copolymers of (1,4)-linked β-D-mannuronic acid (M) and α-L-guluronic acid (G) [22], belonging to a group of polymers used in the food and pharmaceutical industries as modifiers and gelling agents. Numerous studies have been performed to understand the mechanisms and structural features involved in the alginate-gelation processes [23]. It is believed that gel formation is due to specific and strong interactions between long stretches of the G unites and divalent cations such as Ca^{2+} [24, 25]. Dialysis experiment showed that a ratio of 4:1 between the G units and Ca^{2+} cations exists in Ca-alginate gels [26]. This fits well with the egg-box model in which specific Ca-mediated interactions involve only two polymer chains. Two pairs of two consecutive G units, each pair belonging to different polymer chains, are "glued" together through the coordination of a Ca^{2+} cation. It has been proposed that this shape creates pocket-like cavities in which Ca^{2+} cations can be easily accommodated as schematically illustrated in Scheme 1 for the "egg-box" model [27]. This "egg-box" approach has been widely accepted as a general model to describe the gel formation process [28, 29].

On the basis of literature data, we expected that the sodium alginate biopolymer would be a good film-forming material for immobilizing redox proteins on electrode surfaces for studying the direct electrochemistry of the proteins. SA forms stable gels at room temperature in the presence of Ca^{2+} cations, which makes the gels much tight. Polyethylene glycol (PEG) is soluble in aqueous solutions and nontoxic, so we want to use it to enlarge the holes in the gels [30, 31]. We used the method to create porous calcium alginate (CA) for the immobilization of myoglobin (Mb) with PEG as a porogenic agent. The porous Mb-CA films were then fabricated on glassy carbon (GC) electrode surface. In the first step, a mixture of SA solution and PEG solution was cast onto GC electrode, and then a certain volume of calcium chloride ($CaCl_2$) solution was sprayed over the surface of the mixture films under suitable conditions; after evaporation of the solvent, the dried CA films was washed by deionized water and a special porous CA films were formed. The next step, Mb was cast over to the porous CA films on the electrode surfaces and formed the electroactive porous Mb-CA films. The stable porous Mb-CA films modified on GC electrode demonstrated good electroactivity in protein-free buffer, which was originated from protein heme Fe(III)/Fe(II) redox couples. Electrochemical catalytic reductions of O_2, H_2O_2, and NO_2^- were observed at the porous Mb-CA films electrodes, showing potential applications of the films as biosensors and bioreactors. This is the first report of the direct electrochemistry of heme proteins incorporated in biocompatible and electrochemically inert porous CA films.

Experimental section

Chemicals

Horse heart myoglobin (Mb; M_W, 17,800; purity, 90%; type III) was obtained from Sigma. SA was purchased from Tianjin Yuanhang Chemical Corporation. PEG (M_W 4,000) was from Shanghai Chemical Reagents Corporation. Other chemical reagents, including hydrogen peroxide (H_2O_2, 30%), calcium chloride ($CaCl_2$), potassium ferricyanide ($K_3[Fe(CN)_6]$), sodium nitrite ($NaNO_2$), potassium bromide (KBr), sodium dihydrogen phosphate (NaH_2PO_4), sodium acetate (CH_3COONa), citric acid ($C_6H_8O_7$), and boric acid (H_3BO_3), were of analytical grade and used without further purification. The working solutions of $NaNO_2$ and H_2O_2 were freshly prepared before being used.

The buffer solutions were 0.050 M sodium dihydrogen phosphate at pH 7.0 containing 0.10 M KBr. Other supporting electrolytes were 0.050 M sodium acetate, 0.050 M boric acid, or 0.050 M citric acid, all containing 0.10 M KBr. The pHs of buffers were regulated with HCl or NaOH solutions. Solutions were prepared using deionized water which was purified twice successively by ion exchange and distillation.

Fabrication of films

For the electrochemical studies, glassy carbon disk electrodes (Advanced Ceramics, geometric area 0.159 cm^2) were

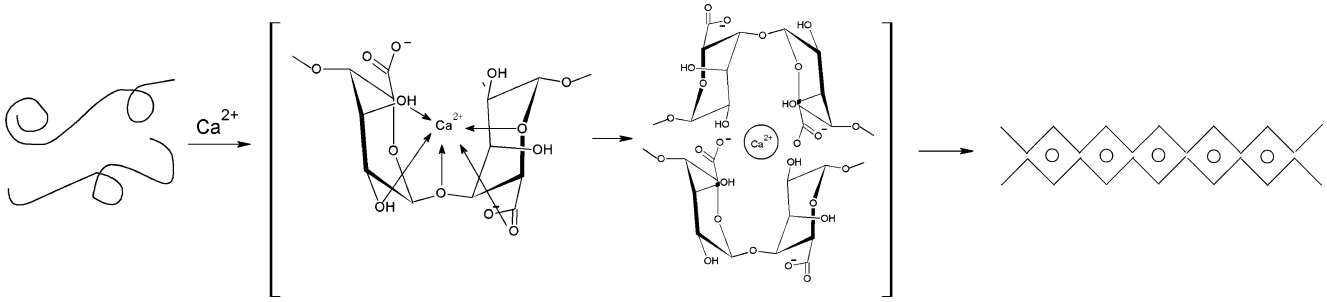

Scheme 1 Schematic illustration of formation of "egg-box" mediated by Ca^{2+} cations

polished with metallographic sandpapers of 1,200 grit, washed with water, and then ultrasonicated in pure water for 30 s.

The preparation of the porous Mb-CA films is as follows. Firstly, 10 μL of a mixture containing four parts of PEG (0.02 g mL^{-1}) solution and one part of SA solution (0.02 g mL^{-1}) was cast on a GC electrode surface. Then, 5 μL of 0.1 g mL^{-1} $CaCl_2$ solution was sprayed over the mixture. A small bottle was fit over the electrode to serve as a closed evaporation chamber so that water evaporated slowly to ensure forming porous CA films. The films were then dried and washed thoroughly using deionized water. Then, 5 μL of 1 mg mL^{-1} Mb solution was cast onto the porous CA films. A small bottle was fit tightly over the electrode so that water evaporated gradually. The porous Mb-CA films were then dried in air overnight before measurement.

The preparation of these samples for different experiments was similar to that described above for the porous Mb-CA films and shown as below. The resulting films with different contents are designated as SA, Mb-SA, CA, and the porous CA films.

SA films were made by only spreading a few tens of microliters of the SA solution (0.02 g mL^{-1}) on the GC electrode and followed by drying. For assembling Mb-SA films, 10 μL of 0.02 g mL^{-1} SA solution was spread on GC electrode surface with a microsyringe. A small bottle was fit over the electrode as a closed chamber. The films were left to dry for about 8 h. Then, 5 μL of 1 mg mL^{-1} Mb solution was cast onto the dry SA films surface. The Mb-SA films were dried 12 h before measurement.

While a certain volume of SA solution without mixing with PEG solution was spread onto GC electrode, an equivalent volume $CaCl_2$ solution was sprayed on the surface of SA solution. It would form the ordinary CA films. The porous CA films were prepared by spraying $CaCl_2$ solution over the mixture surface of SA and PEG on GC electrode.

Sample characterization

Scanning electron microscopy (SEM) measurements were conducted on a JSM-6390LV at an acceleration voltage of 20 kV. The preparation of the film samples was similar to that described above but to use a conductive glass (1× 1 cm) as the substrate. Ultraviolet–visible (UV–vis) spectra were collected on a TU-1901 spectrophotometer. A quartz slide (0.8×4 cm, 1-mm thick) was used as the substrate for supporting the films as described for the preparation of the films on the GC electrode. Nitrogen adsorption/desorption isotherms were measured on a Tristar 3,000 automatic specific surface area and porosity analyzer. The Brunauer–Emmett–Teller (BET) surface area was calculated from the adsorption isotherm in the relative pressure range of 0.05–0.2, while the average pore size was estimated using the Barrett−Joyner−Halenda method.

Electrochemical measurements

A CHI 760 electrochemical workstation (CH Instruments) was used for cyclic voltammetry (CV), square-wave voltammetry (SWV), and alternating current impendence (AC impendence) measurements. A conventional three-electrode cell was used with a saturated calomel electrode (SCE) as the reference electrode, a platinum wire as the counter electrode, and a GC disk with the films as the working electrode. Voltammetries of the porous Mb-CA films were performed in buffers without Mb. Buffers were purged with highly purified nitrogen for about 10 min before use. The measurement was conducted under nitrogen environment. In the CV measurement, measured volumes of air were injected through solution via a syringe in a sealed cell, which had been previously degassed with purified nitrogen. All experiments were done at ambient temperature of 18±2 °C. The porous Mb-CA films electrode were stored in a refrigerator at 4 °C.

Results and discussion

Nitrogen sorption isotherm of films

The nitrogen adsorption desorption data of the samples are summarized in Table 1. Values obtained by the same

Table 1 The data of nitrogen adsorption desorption isotherm for different films

Films	BET area (m^2 g^{-1})	Pore volume (cm^3 g^{-1})	Pore size (nm)
Porous CA	1.9	0.018	12.6
CA	0.35	0.0014	–
SA	–	–	–

The analysis bath temperature was 77.5 K

(–) No data, it cannot be found by experiment at the same condition

method for SA, CA, and the porous CA films are also listed for comparison. The average pore size of the porous CA films calculated from N_2 adsorption/desorption isotherms was 12.6 nm, suggesting a very large uniform mesopore. The BET surface area and the pore volume were calculated to be about 1.9 m^2 g^{-1} and 0.018 cm^3 g^{-1}, respectively, which were larger than that from the ordinary CA films 0.35 m^2 g^{-1} and 0.0014 cm^3 g^{-1} (Table 1). These results indicated the importance of using Ca^{2+} and PEG in the process of making the porous CA films. A non-porous structure of CA film was obtained with the absence of Ca^{2+} and PEG.

This porous CA films exhibits a uniform pore size centered at about 12.6 nm, which is suitable for anchoring Mb molecules (2.5×3.5×4.5 nm) [32], and a high BET surface area (1.9 m^2 g^{-1}), which may greatly enhance the active surface area available for protein immobilization.

As a natural ionic polysaccharide, alginates behave like flexible coils [33]. Upon interaction with divalent cations such as Ca^{2+}, a CA gelation will be formed through the chain–chain association with calcium ions. The amorphous three-dimensional structures of CA gelation are stabilized mainly by hydrogen bondings, intermolecular forces, and coordination bondings [34]. In this study, PEG was used as the porogenic agent in the CA gels to form porous structure, because it is well compatible with water and non-toxic polymer. The porous CA films would be good matrices for immobilizing bio-molecules.

SEM images and UV–vis spectra

Figure 1 shows the SEM images of SA, CA, porous CA, and porous Mb-CA films. Different surface morphologies can be seen from the different samples. While SA and CA films did not show a pore structure (Fig. 1a, b), the porous CA films revealed a rough surface with cavities or holes in it (Fig. 1c). The results showed that PEG could make holes in the CA films. After Mb was cast on the porous CA films, the surface of the porous Mb-CA composite films appeared relatively flat and featureless at the same magnification (Fig. 1d). It is understood that the surface of the porous Mb-CA composite films with Mb as the outermost layer is much smoother than that for porous CA films. This suggests that the interactions between the protein and CA governed the morphology of the dry films. Such interactions may also be responsible for retention of the protein in

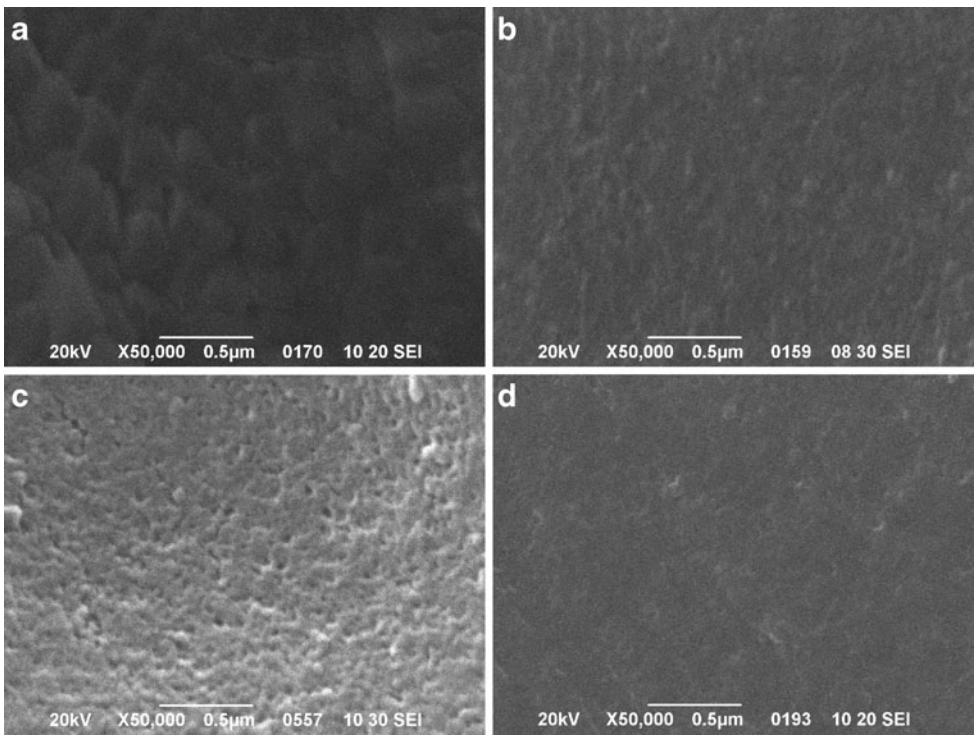

Fig. 1 SEM images of **a** SA films, **b** CA films, **c** porous CA films, and **d** porous Mb-CA films with the same magnification

the films, and the porous structure of CA films may allow the small ions in buffers to go through the films very easily, thus beneficial to the electron transfer of proteins in the films with underlying electrodes.

The position of the Soret absorption band of heme proteins can provide information on the conformation of Mb, especially that in the heme region [35, 36]. The UV–vis data (Fig. 2) confirmed that the Mb in the porous CA films retained its near native conformation. Both dry Mb and the porous Mb-CA films on quartz slides showed the Soret band at 409 nm with a similar peak shape (Fig. 2a, b). The position of the Soret band depended on pH when the porous Mb-CA films were immersed into buffer solutions. At pH between 4.0 and 11.0, the Soret band appeared at 410 nm (Fig. 2c–g), suggesting that the Mb in the films essentially keeps its original structure in the medium pH range. However, after the porous Mb-CA films were immersed in pH 3.0 or 12.0 buffers, the Soret band blue-shifted to 400 nm, and the shape became distorted with smaller peak height (Fig. 2h, i), indicating Mb in the porous CA films may denature to a considerable extent in this relatively extreme pH environment.

Influence of water

A series of porous CA films was made by changing the mass fraction of PEG and the proportion of SA and PEG (mass fraction PEG, 0.01, 0.02, 0.03, 0.04, 0.05, and 0.06; proportion of SA and PEG, 1:1, 1:2, 1:3, 1:4, 1:5, and 1:6). The porous CA films were cast onto glass slides and dried completely in a desiccator. The dried films were clear and transparent. After soaked in water for 24 h, all the films swelled about several times larger than the original dry volume and took on an opaque appearance. The water content of these films was estimated by weighing method. The results showed that the water content remained constant, after immersing the dry films in water for 24 h. Besides, the water content in the porous CA films with different proportion of SA and PEG displayed the same trend; when the proportion of SA and PEG was 1:4, the water content of the porous CA films reached the highest value, estimated to be about 90 wt%. In this report, all of the porous CA films were prepared with the same proportion (1:4).

The measurement of water contents was also used to investigate the influence of PEG in the process of making the porous CA films. For comparison, films of the ordinary CA and the porous CA were prepared at the same condition. The results showed that completely hydrated porous CA films had nearly 90 wt% water contents, making the films as a hydrogel, which was much higher than that of ordinary CA film without PEG (40.6 wt%).

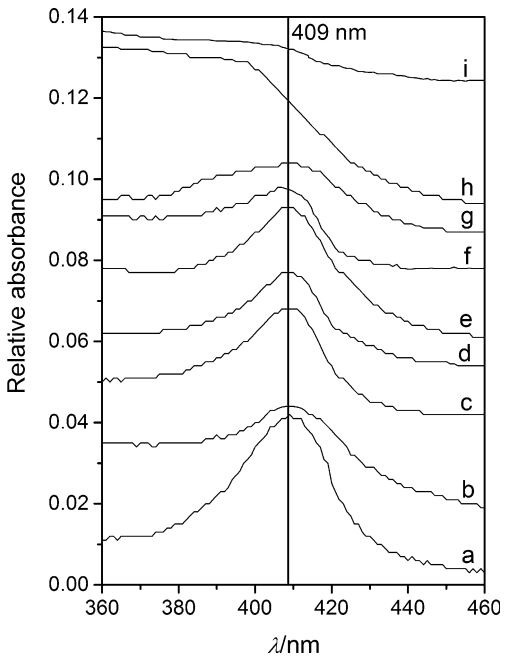

Fig. 2 UV-vis absorption spectra of Mb and porous Mb-CA films on quartz slides for **a** dry Mb film; **b** dry porous Mb-CA film and porous Mb-CA films in different pH buffers: **c** pH 5.0; **d** pH 7.0; **e** pH 9.0; **f** pH 4.0; **g** pH 11.0; **h** pH 3.0; **i** pH 12.0

Alternating current impendence

AC impendence was employed to monitor the properties of the porous CA films with the redox probe of $[Fe(CN)_6]^{3-/4-}$ at its formal potential (0.17 V vs SCE). Figure 3 shows the results of the AC impedance in the form of Nyquist diagrams at the blank GC electrode, porous CA film electrode, CA film electrode, and SA film electrode. The typical semicircle was observed for the films, showing that these films had influences on their AC impendence responses. The diameter of the semicircle usually equals the electron-transfer resistance (R_{ct}), which controls the electron-transfer kinetics of the redox-probe at the electrode interface [37]. The values of R_{ct} were estimated by using the Randles equivalent circuit [38, 39] as the model and fitting the impedance data into the model. The fitted values for the blank GC electrode, porous CA, CA, and SA films were 433.1, 1,433.4, 2,771.5, and 3,315.0 Ω, respectively.

As shown in Fig. 3, there is very low charge transfer resistance for $[Fe(CN)_6]^{3-/4-}$ at bare GC electrode (Fig. 3a). After modifying GC electrode with CA and SA film (Fig. 3c, d), the R_{ct} increased dramatically to 2,771.5 and 3,315.0 Ω, indicating that the ordinary CA and SA films hinder the charge transfer. While the porous CA film was attached to the electrode surface, it can be seen that R_{ct} decreased to about 1,433.4 Ω (Fig. 3b), implying that the porous CA films may play an important role similarly to a conducting wire or electro-conducting tunnel, which makes

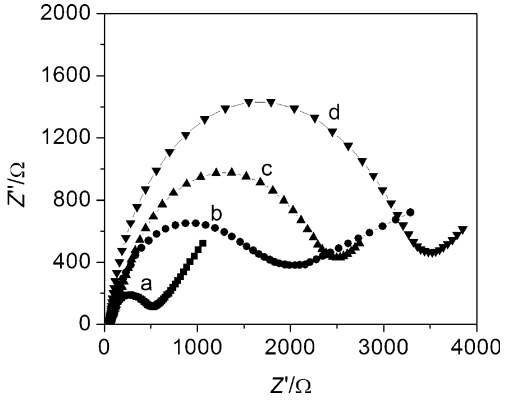

Fig. 3 AC impendence programs of 5 mM $[Fe(CN)_6]^{3-/4-}$ at 0.17 V for **a** black GC electrode, **b** porous CA films, **c** CA films, and **d** SA films on GC electrodes

it easier for the electron transfer to take place [40]. These data showed that the porous CA film have been successfully attached to the electrode surface and formed a tuneable kinetic barrier.

Cyclic voltammetry

When a porous Mb-CA film electrode was immersed into pH 7.0 buffers without Mb, a pair of well-defined and nearly reversible CV peaks at about −0.340 V vs SCE was observed (Fig. 4a), which is characteristic of heme Fe(III)/Fe(II) redox couples [41, 42]. The observed formal potential ($E^{o\prime}$) was obtained by the average of reduction and oxidation peak potentials. The value of $E^{o\prime}$ for Mb in porous Mb-CA films at pH 7.0 was in accordance with previous studies for Mb entrapped in polymer films such as Mb-CS [43] and Mb-AQ films [9]. The separation between the anodic and the cathodic peak potentials ($\Delta E_p = E_{pa} - E_{pc}$ = 66 mV) suggested that the electrochemical process of Mb confined on porous CA film was reversible. As a control

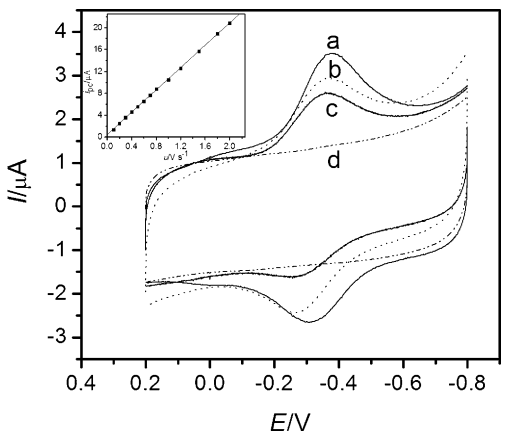

Fig. 4 Cyclic voltammograms at 0.2 V s^{-1} in pH 7.0 buffers for **a** porous Mb-CA films, **b** Mb-SA films, **c** ordinary Mb-CA films, **d** porous CA films. *Inset* Plots of cathodic peak currents vs scan rates

experiment, no CV response in the same potential range was observed on the porous CA film modified GC electrode (Fig. 4d). These observations indicated that the electron transfer between Mb and glassy carbon electrodes was greatly enhanced in porous CA films, which provided a suitable microenvironment for Mb to exchange electron with the underlying GC electrodes.

CV was also used to further investigate the influence of Ca^{2+} and PEG in the process of making the porous CA films, and a comparison was made with Mb-SA, ordinary Mb-CA, and the porous Mb-CA films. The results showed that while two pairs of redox peaks for Mb-SA, ordinary Mb-CA, and porous Mb-CA films were also observed, their peak current were lower than that for the porous Mb-CA films (Fig. 4). From the results shown in the Table 2, in pH 7.0 buffers, Mb-SA and Mb-CA films showed the formal potential ($E^{o\prime}$) at −0.33 and −0.32 V (vs SCE), respectively, while $E^{o\prime}$ of the porous Mb-CA films were at −0.34 V, little negative than the former. The shape of the CV of the Mb-SA and the ordinary Mb-CA films were very similar to those of the porous Mb-CA films, but the separation between the anodic and the cathodic peak potentials ($\Delta E_p = E_{pa} - E_{pc}$) of porous Mb-CA films was smaller than that of the Mb-SA and the ordinary Mb-CA films. Besides, the peak current (I_{pc}) of the porous Mb-CA films was the largest among the three films. These results suggested that porous Mb-CA films displayed the best performance on enhancing the electron transfer between Mb and the electrodes under the same experimental condition, which was consistent with the AC impendence results.

The surface concentration of electroactive proteins (Γ^*) can be estimated by integration of CV reduction peak and applying the equation of $Q = nFA\Gamma^*$ [31], where Q is the charge (C) passing through the electrode with full reduction of electroactive Mb in the films, A is the area of the electrode (0.159 cm^2), and n and F have their usual meaning. The surface concentration (Γ^*) of electroactive Mb for different Mb-films are listed in Table 2 for comparison. The Γ^* values of the porous Mb-CA film was 9.18×10^{-11} mol cm^{-2}. Compared with the total amount of Mb deposited on the electrode surface ($\Gamma=1.76\times10^{-9}$ mol cm^{-2}), the percentage of electroactive Mb was about 5.23%, suggesting that only those Mb molecules closest to the electrode surface can display electrochemical activity. Among the three kinds of Mb-films, porous Mb-CA films demonstrated the largest Γ^* value.

The porous Mb-CA films were tested by CV with different scanning rates. CVs of porous Mb-CA films had symmetric peak shapes and nearly equal heights of reduction and oxidation peaks. The heights of the reduction peak were linearly proportional to scan rates from 0.1 to 2.0 V s^{-1} with correlation coefficient 0.999 (see the inset in

Table 2 The electrochemical parameters for different Mb films on GC electrodes

Films	$E^{o\prime}$ (V vs SCE)	I_{pc} (μA)	ΔE_p (mV)	Γ^* (mol cm^{-2})	Percent of electroactive Mb
Porous Mb-CA	−0.34	1.736	66	9.18×10^{-11}	5.23
Mb-SA	−0.33	1.171	81	4.19×10^{-11}	2.39
Mb-CA	−0.32	1.017	102	3.22×10^{-11}	1.83

$E^{o\prime}$ is the formal potential; I_{pc} is the cathodic peak current; $\Delta E_p = E_{pa} - E_{pc}$ is the separation between the anodic and the cathodic peak potentials; Γ^* is the surface concentration of electroactive Mb in different Mb films modified on electrodes. These Data were estimated by CVs in pH 7.0 buffers

Fig. 4). These results are characteristic of thin-layer electrochemical behavior [44], suggesting that all electroactive MbFe(III) in the films was converted to MbFe(II) on the forward negative scan, with full conversion of MbFe(II) back to MbFe(III) on the reverse positive scan. The total amount of charge passed through the electrode for reduction of electroactive MbFe(III) in the films was essentially independent of the scan rates within the study range.

The pH of the external solution had a great influence on CV peak potentials of porous Mb-CA films. An increase in buffer pH led to a negative shift in potential for both reduction and oxidation CV peaks, accompanied with the change of CV peak shape. In general, all changes in CV peak potentials and currents with pH were reversible between 4.0 and 11.0. For example, CVs for the porous Mb-CA film in pH 5.5 buffer were reproduced after immersion in pH 8.0 buffer and then returning the film to the pH 5.5 buffer. CV data were used to investigate the pH effect on the formal potentials ($E^{o\prime}$). The formal potential ($E^{o\prime}$) had a linear relationship varied linearly with the pH from 4.0 to 11.0 with a slope of −52.7 mV/pH. This value is close to the theoretical value of −57.6 mV/pH at 18 °C for a reversible electron transfer coupled by proton transportation with the equal number of protons and electrons [45, 46]. Thus, the electrode reaction of the porous Mb-CA films can be expressed as below:

$$\mathrm{MbFe(III)} + \mathrm{H^+} + \mathrm{e^-} \rightleftarrows \mathrm{MbFe(II)}$$

An inflection point appeared in the $E^{o\prime}$–pH plot at pH 4.0 for the porous Mb-CA films. At pH<4.0, the variation of $E^{o\prime}$ values with pH showed a much smaller slope, suggesting that protonation of Mb took place below pH 4.0 and the protonatable site of proteins associated with the electrode reaction has an apparent pK_a value of 4.0 [47, 48].

The surface concentration (Γ^*) of electroactive Mb in the film estimated by integration of CV reduction peak was nearly constant between pH 4.0 and 11.0, with an average value of 8.93×10^{-11} mol cm^{-2}. However, it decreased by about 18.46% when the pH was shifted from 4 to 3, indicating the influence of pH on the amount of electroactive Mb in the porous Mb-CA films.

The stability of the porous Mb-CA films was tested by CV with two different methods. In the solution study, GC electrodes coated with the porous Mb-CA films were stored in pH 7.0 blank buffers, and CV tests were carried out periodically. Alternately, with a "dry method," the porous Mb-CA film electrodes were kept in dry form in air for most of the storing time and just returned to buffers occasionally for CV measurements. With both methods, the porous CA films showed excellent stability. The peak potentials and currents essentially remained unchanged for at least 1 month.

Square-wave voltammetry

SWV has better signal/noise ratio and resolution, as a pulse electrochemical method, is easier to analyze theoretically and quantitatively than those sweep methods such as CV [49], although CV is useful for determination of electron transfer constant. SWV was used here to estimate the average apparent heterogeneous electron transfer rate constant (k_s) and other electrochemical parameters for Mb in the porous CA films. The procedure involved nonlinear regression analysis for SWV forward and reverse curves using a model that combines a single-species thin-layer SWV model with an $E^{o\prime}$ dispersion model as described in the literature [47, 50].

Since the SWV model of a single electroactive species with thin-layer electrochemical behavior [51] did not fit the experimental voltammograms for the porous Mb-CA films [6], a model combined dispersion of $E^{o\prime}$ values with the single-species SWV model was used to fit the data here [47, 50], in which the SWV current (I) is

$$I = \sum_{j=1}^{p} I_j$$

where I_j is the contribution of the jth of p classes of redox centers with formal potentials $E_j^{\circ\prime}$ to the total current.

All nonlinear regression analyses were done with a program based on the Marquardt–Levenberg algorithm, assuming absolute errors in dependent variables [52]. It is important to realize the limitations of the above model,

especially in interpreting the estimated k_s, which is an apparent rate constant. The model assumes diffusionless, thin-layer electrochemical conditions. It neglects rate limiting ion entry or ejection, electron self-exchange, and molecular interactions within the films. Thus, k_s obtained by this method is probably best interpreted as a measure of the rate of the overall electron transfer process dependent on film and electrode properties. It is suitable for between-film comparisons only.

Preliminary studies showed that the $E^{o'}$ dispersion model with $p=5$ gave a reasonable compromise between acceptable goodness of fit, consistency of parameters, and time of computation. A similar conclusion was found for SWV data on films of Mb-AQ [9] and Mb surfactants [47, 50]. Thus, the $p=5$ model was used here. Each value of k_s and $E^{o'}$ reported is the average of analysis of six or more SWVs from which background had been subtracted.

An analysis of the SWV data for porous Mb-CA films showed a good fit to the $5-E^{o\prime}$ dispersion thin-layer SWV model in the range of various amplitudes and frequencies (Fig. 5). Frequency ranges were chosen in which the kinetic influence on the data was sufficient to obtain k_s with minimum standard error [52]. The average value of k_s obtained from the fittings at pH 7.0 was 28.18 s^{-1} with $E^{o\prime}$ as −0.339 V vs SCE. The value of $E^{o\prime}$ from CV data was −0.340 V vs SCE. The value of $E^{o\prime}$ obtained from the fitting was similar with the data from the CV calculation. The k_s value of the porous Mb-CA films is in the same order as that of other Mb films [43, 53], qualitatively in agreement with the quasi-reversible CV behavior of thin films. The $E^{o\prime}$ value obtained from the fitting for the porous Mb-CA films is close to that estimated by CV, but different from that for Mb in other types of films. This indicates that the film microenvironment and film components may influence the $E^{o\prime}$ value [6].

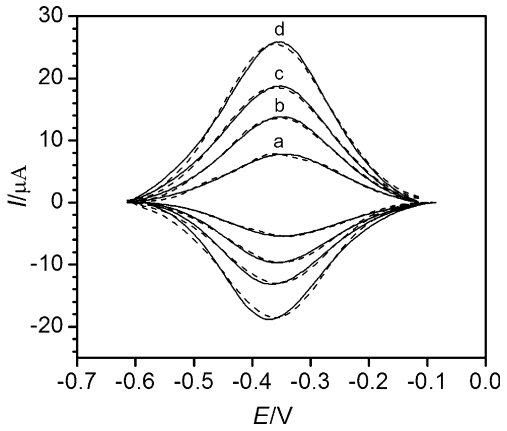

Fig. 5 Square wave forward and reverse current voltammograms for the porous Mb-CA films in pH 7.0 buffers at different frequencies. *Dashed lines* represent the experimental SWV from which the background has been subtracted. The *solid lines* are the best fit obtained by nonlinear regression onto the $5-E^{o\prime}$ dispersion model. SWV condition: pulse height, 75 mV; step height, 4 mV; and frequencies (Hz), **a** 50, **b** 100, **c** 150, and **d** 190

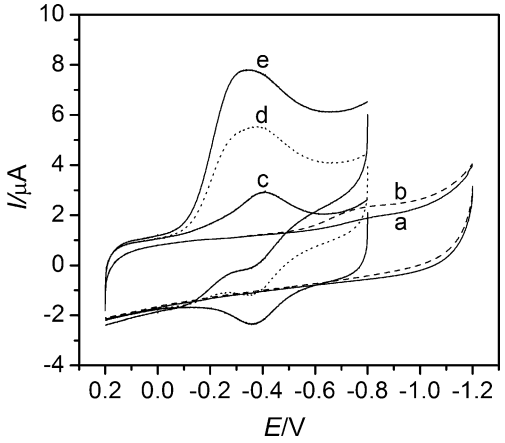

Fig. 6 Cyclic voltammograms at 0.1 V s^{-1} in 8 mL of pH 7.0 buffers for **a** porous CA films with no oxygen present, **b** porous CA films after 10 mL of air was injected into a sealed cell, **c** porous Mb-CA films with no oxygen present, **d**, **e** porous Mb-CA films after 5 mL, 10 mL of air was injected respectively

Electrocatalytic reactivity

Electrochemical catalytic reduction of oxygen by the porous Mb-CA films was examined using the CV technique. When a certain amount of air was passed through pH 7.0 buffers by a syringe, a significant increase in reduction peak at about −0.4 V was observed. This increase in reduction peak was accompanied by the disappearance of the oxidation peak for MbFe(II). An increase in the amount of oxygen in solution increased the reduction peak current (Fig. 6). For porous CA films with no Mb incorporated, the peak for direct reduction oxygen was observed at about −0.80 V. Thus, porous CA films decreased the reduction overpotential of oxygen by at least 0.5 V.

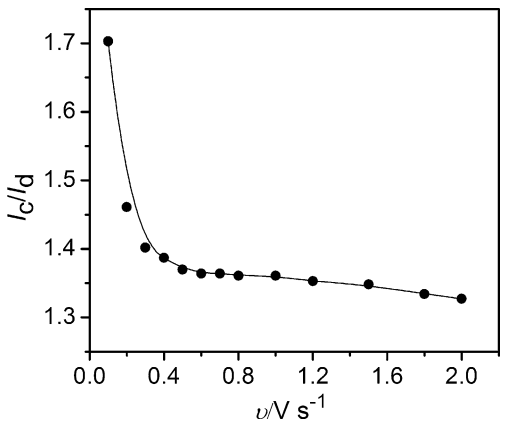

Fig. 7 Influence of scan rate on catalytic efficiency, I_c/I_d, for porous Mb-CA films in 8 mL pH 7.0 buffers, where I_d is the CV reduction peak current in buffer without oxygen and I_c is the CV reduction peak current with 20 mL of air injected

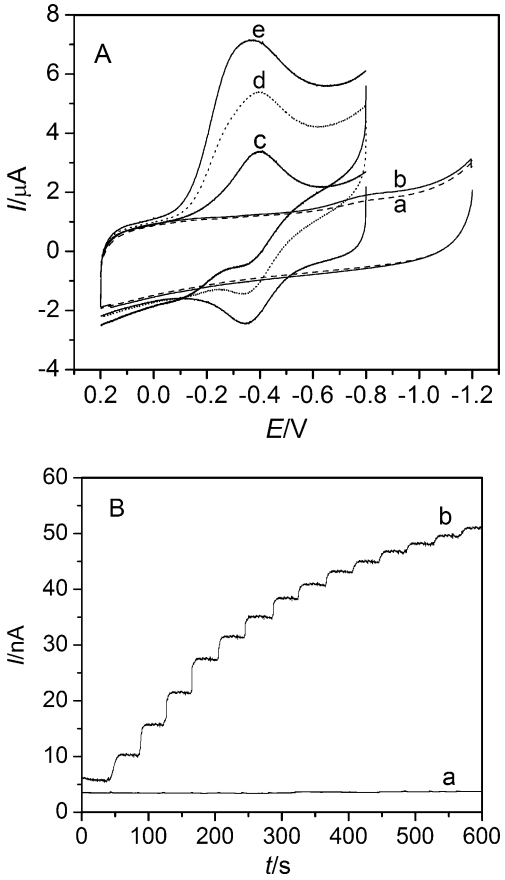

Fig. 8 **a** Cyclic voltammograms at 0.1 V s^{-1} in 8 mL of pH 7.0 buffers for **a** porous CA films with no H_2O_2 present, **b** porous CA films with 0.025 mM H_2O_2 present, **c** porous Mb-CA films with no H_2O_2 present, **d** porous Mb-CA films with 0.025 mM H_2O_2 present, **e** porous Mb-CA films with 0.05 mM H_2O_2 present. **b** Amperometric response of **a** porous CA films and **b** porous Mb-CA films at −0.1 V in pH 7.0 buffers solution with 0.025 mM H_2O_2 injected every 40 s

Catalytic efficiency, expressed as a ratio of reduction peak current of porous Mb-CA films in the presence (I_c) and absence (I_d) of oxygen, I_c/I_d, decreased with the increase of scan rate (Fig. 7), also characteristic of electrochemical catalysis [54].

Catalytic CV behavior was also observed for hydrogen peroxide at porous Mb-CA films, which is very similar to that of the oxygen system. When H_2O_2 was added to pH 7.0 buffers, an increase in reduction peak at about −0.36 V was observed (Fig. 8a), accompanied by a disappearance of the oxidation peak for MbFe(II). However, no direct reduction peak was observed on blank porous CA films in the presence of H_2O_2 in the studied potential range.

With the porous Mb-CA films, the catalytic reduction peak potential for hydrogen peroxide was almost the same as that for oxygen (Figs. 6 and 8a), indicating the similarity of mechanism between the two systems. Reactions of hydrogen peroxide with Mb can be exemplified by the following equation [55]:

$$\mathrm{MbFe(III)} + \mathrm{H_2O_2} \rightarrow \mathrm{Compound\ I} + \mathrm{H_2O} \quad (1)$$

$$\mathrm{Compound\ I} + \mathrm{H_2O_2} \rightarrow \mathrm{MbFe(III)} + \mathrm{O_2} \quad (2)$$

$$\mathrm{MbFe(III)} + \mathrm{e^-} \rightarrow \mathrm{MbFe(II)\ at\ electrode} \quad (3)$$

$$\mathrm{MbFe(II)} + \mathrm{O_2} \rightarrow \mathrm{MbFe(II)} - \mathrm{O_2\ fast} \quad (4)$$

$$\mathrm{MbFe(II)} - \mathrm{O_2} + 2\mathrm{e^-} + 2\mathrm{H^+} \rightarrow \mathrm{MbFe(II)} + \mathrm{H_2O_2\ at\ electrode} \quad (5)$$

There are two catalytic cycles here: MbFe(II) reacts with O_2 and forms MbFe(II)–O_2 in Eq. 4, and produced MbFe (II)–O_2 will receive two electrons at electrodes and return to MbFe(II) again in Eq. 5; H_2O_2 produced in Eq. 5 will participate in Eq. 1 or 2 to produce dioxygen, which will then induce or promote the catalytic cycle of Eqs. 4 and 5.

The electrocatalytic reduction of H_2O_2 at porous Mb-CA films was also tested by amperometry. Figure 8b illustrated a typical amperometric response of porous Mb-CA films with the stepwise addition of H_2O_2 at the constant potential of −0.1 V vs SCE. The stepped increase of H_2O_2 concentration in buffers caused the corresponding growth of catalytic reduction currents with a linear relationship of 25–100 μM for porous Mb-CA films. In contrast, at protein-free porous CA film electrodes, no current response was observed after the addition of H_2O_2.

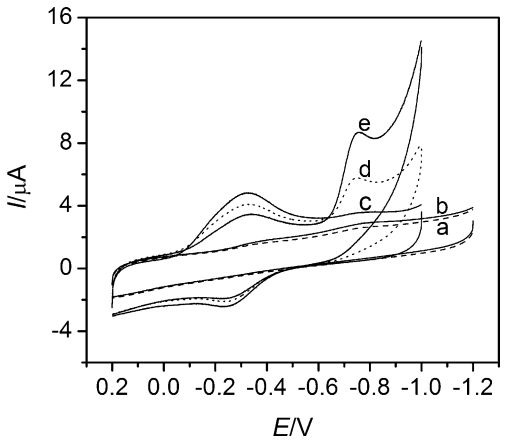

Fig. 9 Cyclic voltammograms at 0.1 V s^{-1} in pH 5.0 buffers for **a** porous CA films in buffers containing no $NaNO_2$, **b** porous CA films in buffers containing 5 mM $NaNO_2$, **c** porous Mb-CA films in buffers containing no $NaNO_2$, **d** porous Mb-CA films in buffers containing 5 mM $NaNO_2$, and **e** porous Mb-CA films in buffers containing 10 mM $NaNO_2$

Under acidic conditions, the NO_2^- species underwent a disproportionation reaction. One of the products was NO, which can form MbFe(II)–NO with Mb. Lin and co-workers [56] studied the electrocatalytic reduction of NO_2^- with Mb-DDAB films on PG electrodes and observed similar results. It was because that MbFe(II)–NO was reduced in the electrode surface. When NO_2^- was added into the pH 7.0 buffers, a catalytic peak was observed at about −0.73 V. The peak current increased with the concentration of NO_2^- (Fig. 9). The linear relationship of the electrocatalytic reduction peak current and NO_2^- concentration was observed between 1.5 and 25 mM with a correlation coefficient of 0.997. Direct reduction of NO_2^- on porous CA films without Mb was not found. Using this property, we can detect the NO_2^- indirectly.

The operational stability of the porous Mb-CA films was examined with intermittent measuring the current response to 0.5 mM H_2O_2 in the stirred buffers every 8 h for 15 days. The results showed the remaining activities of Mb related to the initial Mb activity. The sensor was stored in buffers in a refrigerator at 4 °C when not in use. The catalytic current response maintained about 79% of the initial signal within 15 days of storage. The 25 μM H_2O_2 solution was then determined with five electrodes fabricated independently, and the relative standard deviation was 1.86% (from measurement of anodic peak currents). The results indicate that the modified electrode has excellent operational stability and reproducibility in both the preparation procedure and the voltammetric determinations with good long-term stability.

Conclusions

The porous Mb-CA films were prepared using a two-step method. One was the preparation of porous calcium alginate films, while the other one was to incorporate Mb into the porous CA films on various solid surfaces. The results of nitrogen sorption, SEM, AC impendence, and CV indicated that the porous CA films were obtained in the presence of polyethylene glycol as a porogenic agent. The porous structure of the films enables CA a good matrix for immobilizing biomacromolecules. The pore diameter was about 12.6 nm. Completely hydrated porous CA films had nearly 90 wt% water contents, making the films as a hydrogel, thus providing a favorable microenvironment for the electron exchange between Mb and the electrode. UV–vis results showed that Mb in the porous films retained its near native configuration at medium pH. This may greatly contributed to the good electroactivity of Mb in the porous films. Cyclic voltammetry results showed a pair of well-defined redox peaks of Mb. Moreover, the stable porous Mb-CA films also demonstrated good electrocatalytic properties toward different substrates of environmental or biological significance, such as O_2, H_2O_2, and NO_2^-. The electrode modified with the porous Mb-CA films was found to exhibit good operational and storage stability, reproducibility and fast response time for H_2O_2 detection. This novel approach that combines the preparation of porous CA films with the fabrication of Mb on electrodes may provide a new approach to realizing the direct electrochemistry of proteins. This kind of protein films also provides opportunities for developing biosensors based on direct or mediator-free electrochemistry of proteins.

Acknowledgment The Taishan Scholars Program of Shangdong Province, the financial support of the Qingdao University Science Foundation, and the Growing Base for State key Laboratory of Qingdao University are gratefully acknowledged.

References

1. Wilson G (1987) In: Turner A (ed) Biosensors, 3rd edn. New York, Oxford University
2. Chaplin MF, Bucke C (1990) Enzyme technology. Cambridge University, Cambridge
3. Gorton L, Lindgren A, Larsson T, Munteanu FD, Ruzgas T, Gazaryan I (1999) Anal Chim Acta 400:91–108
4. Armstrong FA, Heering HA, Hirst J (1997) Chem Soc Rev 26:169–179
5. Sucheta A, Ackrell BAC, Cochran B, Armstrong FA (1992) Nature 356:361–362
6. Rusling JF (1998) Acc Chem Res 31:363–669
7. Hu N (2001) Pure Appl Chem 73:1979–1991
8. Yang J, Hu N (1999) Bioelectrochem Bioenerg 48:117–127
9. Hu N, Rusling JF (1997) Langmuir 13:4119–4125
10. Yang J, Hu N, Rusling JF (1999) J Electroanal Chem 463:53–62
11. Sun H, Hu N, Ma H (2000) Electroanalysis 12:1064–1070
12. Sun H, Ma H, Hu N (1999) Bioelectrochem Bioenerg 49:1–10
13. Hu Y, Hu N, Zeng Y (2000) Talanta 50:1183–1195
14. Wang L, Hu N (2001) J Colloid Interface Sci 236:166–172
15. Liu H, Wang L, Hu N (2002) Electrochim Acta 47:2515–2523
16. Chen X, Hu N, Zeng Y, Rusling JF, Yang J (1999) Langmuir 15:7022–7030
17. Zhou Y, Hu N, Zeng Y, Rusling JF (2002) Langmuir 18:211–219
18. Christenson L, Dionne K, Lysaught M (1993) In: Goosen MFA (ed) Fundamentals of animal cell encapsulation and immobilization. Boca Raton, CRC
19. Blandino A, Macías M, Cantero D (2000) Enzyme Microb Technol 27:319–324
20. Zhao H, Zheng W, Meng Z, Zhou H, Xu X, Li Z, Zheng Y (2009) Biosens Bioelectron 24:2352–2357
21. Sun W, Wang D, Gao R, Jiao K (2007) Electrochem Commun 9:1159–1164
22. Blandino A, Macías M, Cantero D (1999) J Biosci Bioeng 88:686–689
23. Moe S, Draget KI, Skjåk-Bræk G, Smidsrød O (1995) In: Stephen A (ed) Food polysaccharides and their applications. New York, Marcel Dekker
24. Draget KI, Skjåk-Bræk G, Smidsrød O (1997) Int J Biol Macromol 21:47–55
25. Donati I, Holtan S, Morch YA, Borgogna M, Dentini M, Skjåk-braek G (2005) Biomacromolecules 6:1031–1040

26. Morris ER, Rees DA, Thom D, Boyd J (1978) Carbohydr Res 66:145–198
27. Grant GT, Morris ER, Rees DA, Smith PJC, Thom D (1973) FEBS Lett 32:195–198
28. Sikorski P, Mo F, Skjåk-Bræk G, Stokke BT (2007) Biomacromoleculaes 8:2098–2103
29. Braccini I, Pérez S (2001) Biomacromolecules 2:1089–1096
30. Wu L, Ding J (2004) Biomaterials 25:5821–5830
31. Ko HF, Sfeir C, Kumta PN (2007) Mater Sci Eng C 27:479–483
32. Kendrew J, Phillips D, Stone V (1960) Nature 185:422–427
33. Draget KI, Taylor C (2011) Food Hydrocolloids 25:251–256
34. Wang L, Shelton RM, Cooper PR, Lawson M, Triffitt JT, Barralet JE (2003) Biomaterials 24:3475–3481
35. Theorell H, Ehrenberg A (1951) Acta Chem Scand 5:823–848
36. George P, Hanania GIH (1953) Biochem J 55:236–243
37. Katz E, Willner I (2003) Electroanalysis 15:913–947
38. Bard AJ, Faulkner LR (2000) Electrochemical method: fundamentals and applications. Wiley, New York
39. Randles JEB (1947) Discuss Faraday Soc 1:11–19
40. Zhao J, Henkens RW, Stonehuerner J, O'Daly JP, Crumbliss AL (1992) J Electroanal Chem 327:109–119
41. Chen X, Xie H, Kong J, Deng J (2001) Biosens Bioelectron 16:115–120
42. Zhang Z, Chouchane S, Magliozzo RS, Rusling JF (2002) Anal Chem 74:163–170
43. Huang H, Hu N, Zeng Y, Zhou G (2002) Anal Biochem 308:141–151
44. Murray RW (1984) In: Bard AJ (ed) Electroanalytical chemistry. New York, Marcel Dekker
45. Meites L (1965) Polarographic techniques. Wiley, New York
46. Bond AM (1980) Modern polarographic methods in analytical chemistry. Marcel Dekker, New York
47. Nassar A-EF, Zhang Z, Hu N, Rusling JF, Kumosinski TF (1997) J Phys Chem B 101:2224–2231
48. Yang A-S, Honig B (1994) J Mol Biol 237:602–614
49. Osteryoung JG, O'Dea JJ (1986) In: Bard AJ (ed) Electroanalytical chemistry. New York, Marcel Dekker
50. Zhang Z, Rusling JF (1997) Biophys Chem 63:133–146
51. O'Dea JJ, Osteryoung J (1993) Anal Chem 65:3090–3097
52. Rusling JF, Kumosinski TF (1996) Nonlinear computer modeling of chemical and biochemical data. Academic, New York
53. He P, Hu N, Rusling JF (2004) Langmuir 20:722–729
54. Andrieux CP, Blocman C, Dumas-Bouchiat JM, M'Halla F, Savéant JM (1980) J Electroanal Chem 113:19–40
55. Huang R, Hu N (2001) Bioelectrochemistry 54:75–81
56. Lin R, Bayachou M, Greaves J, Farmer PJ (1997) J Am Chem Soc 119:12689–12690